THE JOURNAL OF PHYSICAL CHEMISTRY C

Article

Cite This: J. Phys. Chem. C 2019, 123, 18455−18466

pubs.acs.org/JPCC

Thermal Atomic Layer Etching of Al_2O_3, HfO_2, and ZrO_2 Using Sequential Hydrogen Fluoride and Dimethylaluminum Chloride Exposures

Published as part of The Journal of Physical Chemistry virtual special issue "Hai-Lung Dai Festschrift".

Younghee Lee and Steven M. George*

Department of Chemistry, University of Colorado, Boulder, Colorado 80309, United States

ABSTRACT: Atomic layer etching (ALE) of Al_2O_3, HfO_2, and ZrO_2 was accomplished using sequential exposures with hydrogen fluoride (HF) as the fluorination reagent and dimethylaluminum chloride (DMAC, $AlCl(CH_3)_2$) as the metal reactant for ligand exchange. DMAC could provide either CH_3 or Cl ligands for the ligand-exchange reaction. The presence of the Cl ligand on DMAC led to efficient HfO_2 and ZrO_2 etching attributed to the formation of stable and volatile chloride species. *In situ* quartz crystal microbalance (QCM) measurement observed mass changes during Al_2O_3, HfO_2, and ZrO_2 ALE reactions at 200−300 °C. Al_2O_3, HfO_2, and ZrO_2 were etched linearly versus number of HF and DMAC sequential exposures. The QCM analysis confirmed that the HF and DMAC reactions were self-limiting versus reactant exposure. The QCM studies observed mass changes per cycle (MCPC) of −12.2 ng/(cm^2 cycle), −94.1 ng/(cm^2 cycle), and −75.6 ng/(cm^2 cycle) for Al_2O_3, HfO_2, and ZrO_2 ALE, respectively, at 250 °C. These MCPC correspond to Al_2O_3, HfO_2, and ZrO_2 etch rates of 0.39 Å/cycle, 0.98 Å/cycle, and 1.33 Å/cycle, respectively. In comparison, the AlF_3, HfF_4, and ZrF_4 surface layers were estimated to have thicknesses of 3.0 Å, 3.3 Å, and 4.4 Å on Al_2O_3, HfO_2, and ZrO_2, respectively. The magnitudes of these fluoride thicknesses have the same ordering as the etch rates for Al_2O_3, HfO_2, and ZrO_2 ALE, respectively. X-ray reflectivity (XRR) and spectroscopic ellipsometry measurements verified the etch rates for Al_2O_3 ALE. XRR analysis also confirmed smoothening of the etched Al_2O_3 film. The etch rates for Al_2O_3, HfO_2, and ZrO_2 ALE increased with temperature from 200 to 300 °C. A comparison of Al_2O_3, HfO_2, and ZrO_2 ALE using either HF and DMAC or HF and trimethylaluminum (TMA, $Al(CH_3)_3$) revealed that higher etch rates were observed for DMAC for all three materials. Cross-sectional transmission electron microscopy (TEM) studies also revealed that Al_2O_3 ALE on masked Al_2O_3 substrates was isotropic and selective in the presence of SiN and SiO_2. Because of the ability of DMAC to provide either CH_3 or Cl ligands during the ligand-exchange reaction, DMAC should be a very useful metal reactant for the thermal ALE of various materials.

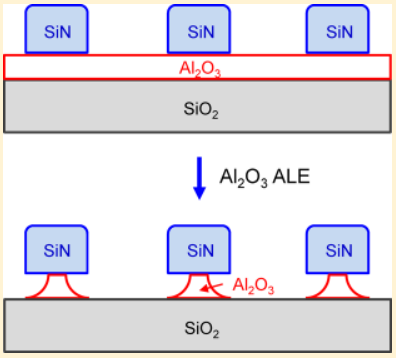

I. INTRODUCTION

Atomic layer etching (ALE) is based on sequential, self-limiting surface reactions that remove a thin film with atomic level precision.[1,2] Plasma ALE processes using sequential halogenation and bombardment by energetic inert ions or neutrals have been developed to accomplish anisotropic etching for >25 years.[1,3,4] In contrast, thermal ALE for isotropic etching has been developed more recently using sequential fluorination and ligand-exchange reactions.[5,6] Thermal ALE is useful to etch materials selectively with atomic layer control without damaging the underlying film.[7]

The first report of thermal Al_2O_3 ALE employed fluorination and ligand-exchange reactions with HF and $Sn(acac)_2$ as the reactants.[6] The thermal ALE proceeds with the formation of a metal fluoride layer and the subsequent removal of the metal fluoride by ligand exchange with a metal reactant.[6,8] The HF and $Sn(acac)_2$ exposure sequence was also able to etch HfO_2, AlF_3, AlN, and ZrO_2.[7,9−11] Another metal reactant, trimethylaluminum (TMA), was used together with HF to etch Al_2O_3 and HfO_2.[7,12,13] $TiCl_4$ was used as the metal reactant together with HF to etch HfO_2 and ZrO_2.[14] The use of different metal reactants for ligand exchange, such as $Sn(acac)_2$, TMA, DMAC, $SiCl_4$, and $TiCl_4$, had demonstrated selective etching of various materials by providing different ligands such as acac, CH_3, and Cl.[7,14]

In the ligand-exchange reaction, the metal reagent accepts F from the metal fluoride and donates a ligand to the metal fluoride.[5,6,8] One metal atom from the metal reagent, M, with ligand, L, and the other metal atom from the metal fluoride, M′, with the fluoride ligand, F, participate in the formation of a four-center transition state.[5] This transition state is stabilized by Lewis acid−base interactions. The M atom in the metal reagent is commonly a Lewis acid. The F in the metal fluoride acts as a Lewis base. F favors the formation of fluoride bridging structures with two metal centers (M−F−M′).[15] Because the M′ atom in the metal fluoride is often a Lewis acid, a ligand

Received: May 20, 2019
Revised: July 3, 2019
Published: July 3, 2019

DOI: 10.1021/acs.jpcc.9b04767
J. Phys. Chem. C 2019, 123, 18455−18466

that can serve as a Lewis base is desirable for ligand transfer. The ligand transfer is favorable when the ligand is capable of forming a bridging structure (M−L−M′).

TMA is one of the most useful metal reagents for Al_2O_3 atomic layer deposition (ALD) due to its high reactivity and high volatility.[16,17] The reactivity and vapor pressure of dimethylaluminum chloride ($AlCl(CH_3)_2$, DMAC) are similar to TMA. The boiling points of DMAC and TMA are nearly the same at 126 and 130 °C, respectively.[18] The use of DMAC for ALE is very promising because both CH_3 and Cl ligands on DMAC are available for ligand exchange. Many metal chlorides in groups 4−6 and groups 13−15 including $AlCl_3$, $HfCl_4$, and $ZrCl_4$ are stable and volatile. Many metal alkyls such as TMA and diethylzinc in groups 12−15 are also stable and volatile. Both stability and volatility are important for the reaction products to leave the surface after the ligand-exchange reaction. Metal reactants having different ligands, such as DMAC, can be versatile for the thermal ALE of various materials.

The Cl ligand has a stronger ability to form a bridging structure (M−L−M′) than the CH_3 ligand. $AlCl_3$ is a solid at room temperature and undergoes sublimation at 180 °C. The dissociation energy for the $AlCl_3$ dimer ($Al_2Cl_6 \leftrightarrow 2AlCl_3$) is E_d = 29.0 kcal/mol.[19] In contrast, $Al(CH_3)_3$ is liquid with boiling point less than 130 °C.[18] The dissociation energy of the TMA dimer ($Al_2(CH_3)_6 \leftrightarrow 2Al(CH_3)_3$) is E_d = 20.2 kcal/mol.[19] DMAC can form a dimeric structure analogous to a four-center transition state during the ligand-exchange reaction because of its Cl ligand. Although both Cl and CH_3 are possible in a bridging structure, Cl in the Al−Cl−Al bridging structure is much more favorable.[20] A dimeric DMAC molecule in the gas phase was confirmed by electron diffraction[20] and mass spectrometry.[21] No measurable dissociation of dimeric DMAC was observed at 92−155 °C.[22] In contrast, TMA shows ∼50% dissociation at 150 °C and exists mostly as a monomer at 215 °C.[19,23]

In this paper, *in situ* quartz crystal microbalance (QCM) measurements examined the thermal ALE of Al_2O_3, HfO_2, and ZrO_2 using sequential exposures of HF and DMAC at 200−300 °C. The etch rates and mass changes during the individual HF and DMAC reactions were investigated during thermal Al_2O_3, HfO_2, and ZrO_2 ALE at different temperatures. X-ray reflectivity (XRR) and spectroscopic ellipsometry analyses were also utilized to measure the film thicknesses versus number of ALE cycles to confirm the etch rates. DMAC was compared with TMA as a metal reactant to understand the role of the Cl ligand in DMAC. Cross-sectional transmission electron microscopy (TEM) studies after Al_2O_3 ALE on masked Al_2O_3 substrates were also employed to determine if thermal Al_2O_3 ALE using HF and DMAC was selective and isotropic.

II. EXPERIMENTAL SECTION

II.A. *In Situ* QCM Studies in a Viscous Flow Reactor. The ALE and ALD reactions were performed in the same viscous flow, hot wall reactor.[6] An *in situ* measurement of the mass change was conducted using a quartz crystal microbalance (QCM) in the reactor.[24] The quartz crystal (gold coated and polished, 6 MHz RC, Colnatec) was placed in a sensor head (BSH-150, Inficon) and sealed with high-temperature epoxy (Epo-Tek H21D, Epoxy technology). The mass changes during the ALE and ALD reactions were measured by a thin-film deposition monitor (Maxtek TM-400, Inficon) with a mass resolution of 0.375 ng/cm^2.[24]

Each reaction temperature at 200, 225, 250, 275, and 300 °C was maintained with a proportional-integral-derivative (PID) temperature controller (2604, Eurotherm) that held the set point temperature to within ±0.04 °C. Change of the temperature required 2 h of stabilization to minimize the effect of temperature fluctuations during the QCM measurements. The pressure in the reactor was monitored by a bakeable capacitance manometer (Baratron 121A, MKS).

A constant flow of 150 sccm of ultra high purity (UHP) N_2 gas into the reactor was regulated by mass flow controllers (Type 1179A, MKS). An additional flow of 20 sccm of N_2 gas defined using a metering bellows-sealed valve (SS-4BMG, Swagelok) prevented deposition on the backside of the QCM crystal. The total N_2 gas flow of 170 sccm produced a base pressure of ∼1 Torr in the reactor. The reactor was pumped by a mechanical pump (Pascal 2015SD, Alcatel).

The Al_2O_3, HfO_2, and ZrO_2 ALE reactions were accomplished using sequential exposures of DMAC (97%, Sigma-Aldrich) and HF derived from HF−pyridine (70 wt % HF, Sigma-Aldrich). The use of HF from the HF−pyridine solution enabled the safer handling of anhydrous HF. Mass spectroscopy has confirmed that a negligible pyridine partial pressure is present over the HF−pyridine solution.[25] A vapor pressure of 90−100 Torr for HF over the HF−pyridine solution has been measured at room temperature.[10] The HF−pyridine solution was transferred to a gold-plated stainless steel bubbler in a dry N_2-filled glovebag. The HF−pyridine and DMAC reactants were maintained at room temperature. DMAC and HF exposures produced pressure transients of 40 mTorr and 80 mTorr, respectively, on top of the base pressure of ∼1 Torr in the reactor.

The Al_2O_3 films were grown on the QCM crystal with Al_2O_3 ALD using TMA (97%, Sigma-Aldrich) and H_2O (Chromasolv for HPLC, Sigma-Aldrich). The HfO_2 and ZrO_2 ALD reactions were conducted using tetrakis(dimethylamido) hafnium (TDMAH, 99.99%, Sigma-Aldrich) and tetrakis-(ethylmethylamido) zirconium (TEMAZ, 99.99%, Sigma-Aldrich,), respectively, together with H_2O.[26] The TMA and H_2O reactants were maintained at room temperature. The bubbler temperatures for TDMAH and TEMAZ were 67 and 112 °C, respectively.[27]

II.B. X-ray Reflectivity and Spectroscopic Ellipsometry. *Ex situ* X-ray reflectivity (XRR) scans were recorded by a high-resolution X-ray diffractometer (Bede D1, Jordan Valley Semiconductors) using Cu Kα (λ = 1.540 Å) radiation. The filament voltage and current in the X-ray tube were 40 kV and 35 mA, respectively. A 10 arcsec step size and a 5 s acquisition time were used for recording all XRR scans with a range of 300−6000 arcsec. The analysis software (Bede REFS, Jordan Valley Semiconductors) fitted the XRR scans to determine film thickness, film density, and surface roughness.

Ellipsometry was performed using a spectroscopic ellipsometer (M-2000, J. A. Woollam) with a range of 240−1700 nm and an incidence angle of 75°. The analysis software (CompleteEASE, J. A. Woollam) determined the thicknesses and refractive index of the film by fitting the Ψ and Δ values based on a Sellmeier model.

For the XRR and ellipsometry studies, Al_2O_3 ALD films were also grown on boron-doped Si(100) wafers (p-type, Silicon Valley Microelectronics). The bare Si substrates were sliced into samples with dimensions of 2.5 cm × 2.5 cm prior

DOI: 10.1021/acs.jpcc.9b04767
J. Phys. Chem. C 2019, 123, 18455−18466

to the Al_2O_3 ALD. These samples were then used as the substrates for the Al_2O_3 ALE studies.

III. RESULTS AND DISCUSSION

III.A. *In Situ* QCM Measurements for Thermal Al_2O_3 ALE. Figure 1 shows the mass change observed by QCM

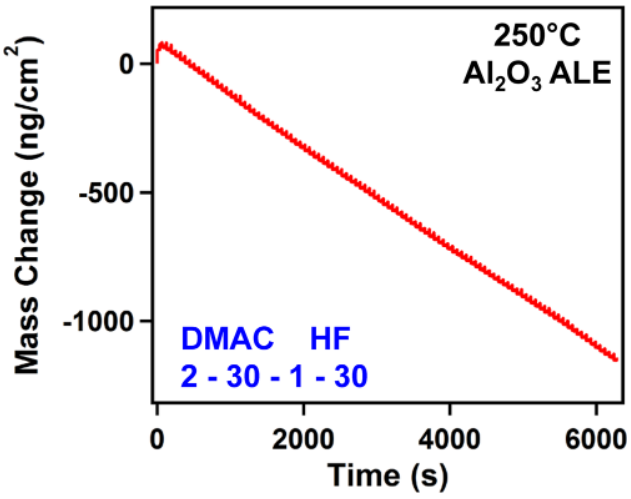

Figure 1. Mass change versus time for Al_2O_3 ALE using sequential DMAC and HF exposures at 250 °C using the reaction sequence of 2−30−1−30.

measurements during 100 cycles of Al_2O_3 ALE at 250 °C using sequential exposures of DMAC and HF. The Al_2O_3 film on the QCM crystal was prepared by 100 cycles of Al_2O_3 ALD using TMA and H_2O at 250 °C. Each ALE cycle was defined by a DMAC dose of 2 s, a first N_2 purge of 30 s, a HF dose of 1.0 s, and a second N_2 purge of 30 s. This reaction sequence is denoted as 2−30−1−30.

The mass change versus time in Figure 1 is linear with a mass change per cycle (MCPC) of −12.2 ng/(cm^2 cycle). This MCPC corresponds to an etch rate of 0.39 Å/cycle based on the Al_2O_3 ALD film density of 3.1 g/cm^3 obtained by XRR measurements. All Al_2O_3 ALE cycles show mass loss except during the first ALE cycle. Mass gains of ΔM_{DMAC} = 54 ng/cm^2 and ΔM_{HF} = 22 ng/cm^2 were observed during the first cycle.

The mass gain for ΔM_{DMAC} during the first DMAC exposure is caused by the formation of $AlCH_3$* and AlCl* surface species on the initial hydroxylated Al_2O_3 substrate. The asterisks designate surface species. HF then reacts with the $AlCH_3$* and AlCl* surface species to form AlF* surface species. HF can also react with the underlying Al_2O_3 film to form an AlF_3 or AlF_xO_y surface layer.[28,29] The fluorination reaction $Al_2O_3 + 6HF \rightarrow 2AlF_3 + 3H_2O$ is thermochemically favorable with a standard free energy change of $\Delta G° = -54$ kcal/mol at 250 °C.[30] This first reaction cycle creates the initial AlF_3 or AlF_xO_y layer on the Al_2O_3 substrate.

Figure 2 displays the mass changes during three sequential Al_2O_3 ALE cycles at 250 °C in the steady state region of Figure 1. Each ALE cycle leads to repeatable mass changes. The DMAC exposure leads to a rapid mass decrease followed by little additional change during the purge time. A mass change of ΔM_{DMAC} = −17 ng/cm^2 was obtained after 2.0 s of DMAC exposure. This mass loss indicates DMAC can remove the AlF_3 or AlF_xO_y surface layer on the Al_2O_3 film. The HF exposure corresponds with a mass gain followed by little change during

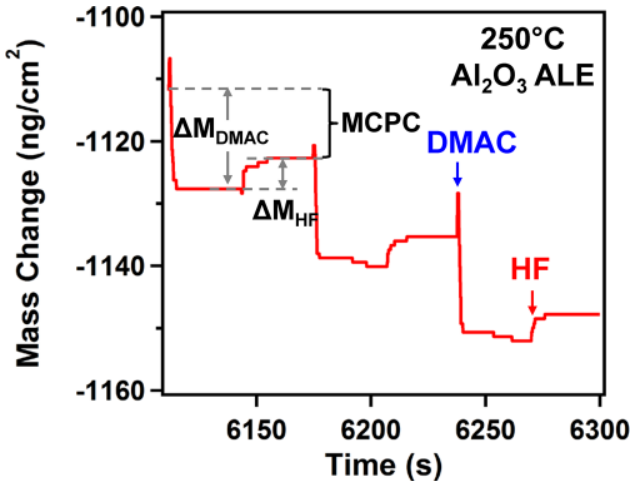

Figure 2. Enlargement of linear region of Figure 1 showing the individual mass changes during the sequential DMAC and HF exposures at 250 °C using the reaction sequence of 2−30−1−30.

the purge time. A mass gain of ΔM_{HF} = 5 ng/cm^2 was observed after 1.0 s of HF exposure. This mass gain is attributed to the reaction of HF with $AlCH_3$* and AlCl* surface species to form AlF* surface species in addition to the fluorination of Al_2O_3 to form an AlF_3 or AlF_xO_y surface layer. This AlF_3 or AlF_xO_y surface layer is again removed by the ligand-exchange reaction during the subsequent DMAC exposure.

Figure 3 shows the MCPC and the ΔM_{DMAC}/MCPC ratio during the 100 cycles of Al_2O_3 ALE at 250 °C shown in Figure 1. The variation in the ΔM_{DMAC}, ΔM_{HF}, and MCPC values is ±0.3 ng/(cm^2 cycle) over the 100 cycles. The ΔM_{DMAC} and ΔM_{HF} mass changes are constant except during the first few cycles. The MCPC is expressed by MCPC = ΔM_{DMAC} +

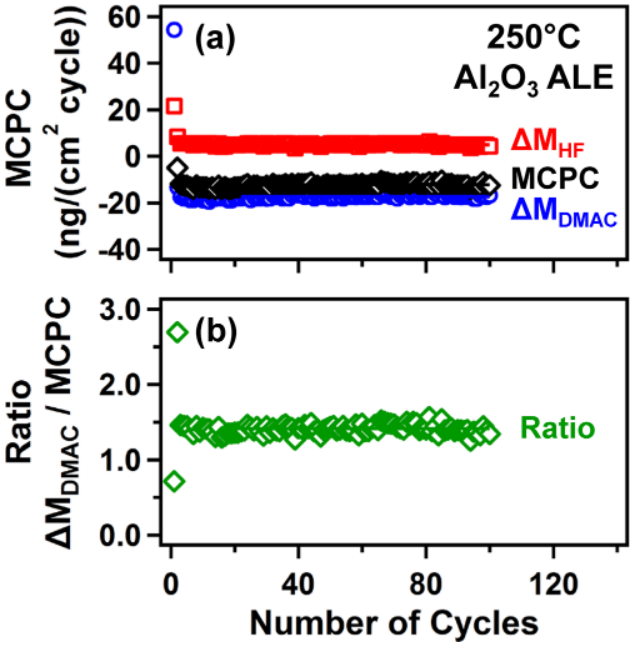

Figure 3. (a) Mass change after the DMAC exposure (ΔM_{DMAC}), mass change after the HF exposure (ΔM_{HF}), and mass change per cycle (MCPC) versus number of ALE cycles at 250 °C. (b) ΔM_{DMAC}/MCPC ratio versus number of ALE cycles.

DOI: 10.1021/acs.jpcc.9b04767
J. Phys. Chem. C 2019, 123, 18455−18466

ΔM_{HF}. Figure 3a displays MCPC, ΔM_{DMAC}, and ΔM_{HF} for the 100 Al_2O_3 ALE cycles at 250 °C. MCPC = −12.2 ng/(cm^2 cycle) was obtained in steady state after a short nucleation period. Figure 3b shows the ΔM_{DMAC}/MCPC ratio during the same 100 Al_2O_3 ALE cycles. A ΔM_{DMAC}/MCPC ratio = 1.4 was obtained in steady state. This ΔM_{DMAC}/MCPC ratio can be used to clarify the mechanism of the Al_2O_3 ALE reaction.[8,10−12,14]

In situ QCM experiments also examined the self-limiting nature of the Al_2O_3 ALE reactions during DMAC and HF exposures at 250 and 300 °C. Figure 4a and 4b show the mass

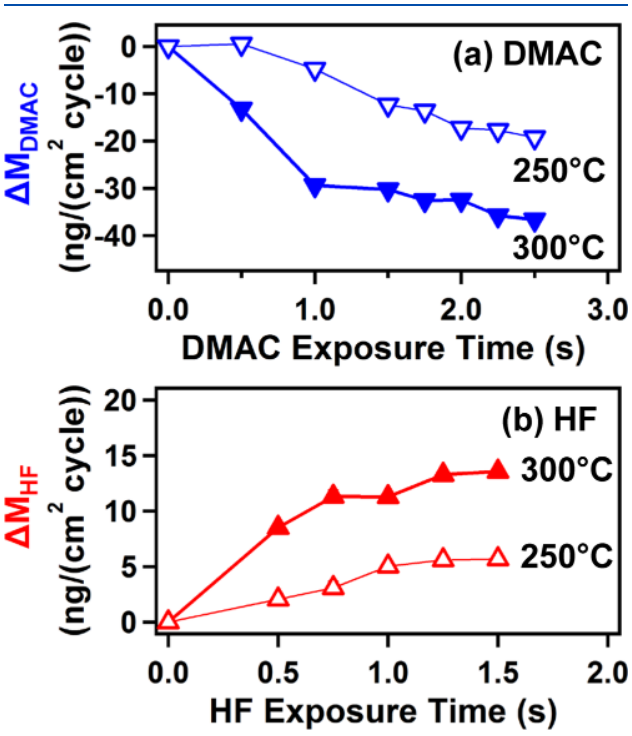

Figure 4. (a) Mass change after DMAC exposure (ΔM_{DMAC}) versus DMAC exposure time at 250 and 300 °C. (b) Mass change after HF exposure (ΔM_{HF}) versus HF exposure time at 250 and 300 °C.

changes monitored as a function of exposure time for DMAC and HF, respectively, at 250 and 300 °C. Figure 4a shows ΔM_{DMAC}, the mass change after the DMAC exposure, with different DMAC exposure times using a single 1.0 s exposure of HF. This reaction sequence can be expressed as x−30−1−30 with constant N_2 purges of 30 s after each reactant exposure. ΔM_{DMAC} decreases versus DMAC exposure time and levels off at longer exposure times.

The mass loss slowly reaches saturation at ΔM_{DMAC} = −17 ng/cm^2 after 2 s of DMAC exposure at 250 °C. This slow self-limiting behavior may indicate the difficulty of complete removal of the AlF_3 or AlF_xO_y surface layer. Additional experiments at 300 °C displayed more pronounced self-limiting behavior. The mass change quickly reaches ΔM_{DMAC} = −30 ng/cm^2 after 1 s of DMAC exposure at 300 °C and approaches saturation after 2.0−2.5 s of DMAC exposure.

Figure 4b shows ΔM_{HF}, the mass change after the HF exposure, with different HF exposure times using a single 2.0 s exposure of DMAC at 250 °C. This reaction sequence can be expressed as 2−30−x−30. ΔM_{HF} versus HF exposure time increases and then levels off at ΔM_{HF} = 5 ng/(cm^2 cycle) after a 1 s HF exposure at 250 °C. This self-limiting behavior is consistent with an AlF_3 or AlF_xO_y surface layer passivating the Al_2O_3 film.[28,29] Additional results for ΔM_{HF} displayed in Figure 4b also confirmed similar self-limiting behavior at 300 °C. The mass gain reaches near saturation at ΔM_{HF} = 11 ng/(cm^2 cycle) after a 0.75 s HF exposure at 300 °C.

Figure 5 displays the mass changes during 100 Al_2O_3 ALE cycles at 200, 225, 250, 275, and 300 °C with the reaction

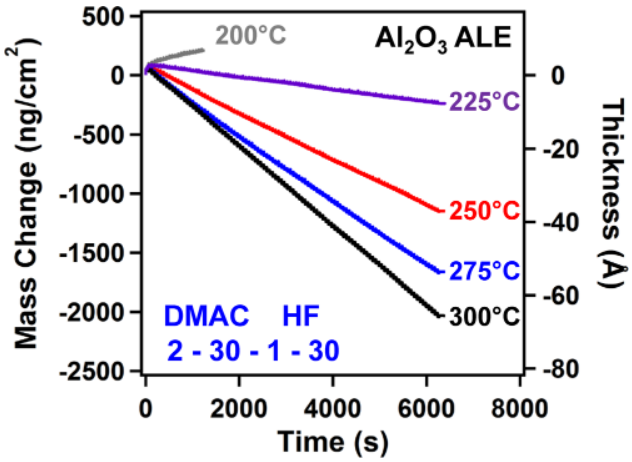

Figure 5. Mass change versus time for Al_2O_3 ALE using sequential DMAC and HF exposures at 200, 225, 250, 275, and 300 °C.

sequence of 2−30−1−30. The initial Al_2O_3 ALD films were grown using 100 cycles of Al_2O_3 ALD at the same temperatures as the ALE reactions. The mass changes versus time during Al_2O_3 ALE show linear etching at 225−300 °C. The MCPC changes with temperature from −3.2 ng/(cm^2 cycle) at 225 °C to −21.3 ng/(cm^2 cycle) at 300 °C. These MCPCs are equivalent to etch rates that increase from 0.10 Å/cycle at 225 °C to 0.69 Å/cycle at 300 °C. These etch rates are again determined using the Al_2O_3 ALD film density of 3.1 g/cm^3.

Figure 5 also shows that a mass gain is observed at 200 °C. This mass gain is attributed to AlF_3 ALD. The growth of AlF_3 using DMAC and HF can be written as $AlCl(CH_3)_2$ + 3HF → AlF_3 + HCl + 2CH_4. Similar results were observed for AlF_3 ALD using TMA and HF as the reactants at T < 225 °C.[25] At temperatures >250 °C, the same TMA and HF reactants yield Al_2O_3 ALE.[25]

The mass changes during the first two Al_2O_3 ALE cycles were investigated to understand the surface species after the sequential DMAC and HF exposures on the hydroxylated Al_2O_3 film. Figure 6 displays an enlargement of the mass changes during the first two Al_2O_3 ALE cycles at the different temperatures in Figure 5. The first DMAC exposure in Figure 6 displays mass gains of ΔM_{DMAC} = 47−56 ng/cm^2 at 200−300 °C. These mass gains are attributed to the reaction of DMAC with AlOH* surface species and described by AlOH* + $AlCl(CH_3)_2$ → $AlOAlCl^*(CH_3)^*$ + CH_4. The mass gains during DMAC exposures are higher than ΔM_{TMA} = 27−32 ng/cm^2 observed during TMA exposure on initial hydroxylated Al_2O_3 films at 250−325 °C.[12] These higher mass gains are consistent with the presence of AlCl* species, in addition to $AlCH_3$* species, when using DMAC.

The first HF exposure in Figure 6 displays mass gains of ΔM_{HF} = 20−22 ng/cm^2 at 200−300 °C. These mass gains

DOI: 10.1021/acs.jpcc.9b04767
J. Phys. Chem. C 2019, 123, 18455−18466

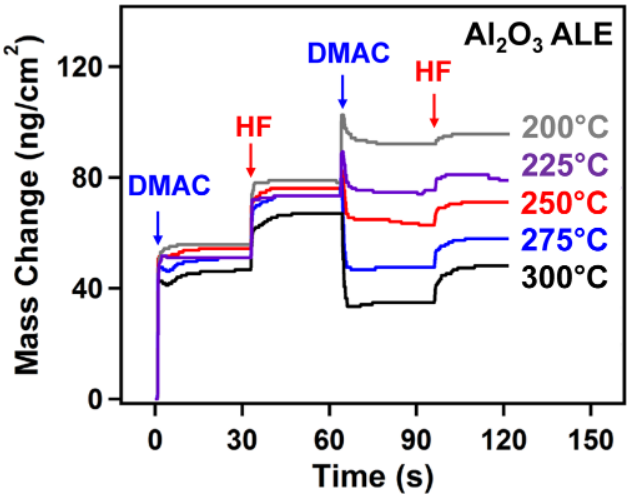

Figure 6. Enlargement of the first two ALE cycles in Figure 5 showing the individual mass changes during the sequential DMAC and HF exposures at 200, 225, 250, 275, and 300 °C.

during the first HF exposure result from the reaction of HF with $AlCH_3$* and AlCl* species in addition to the fluorination of the Al_2O_3 substrate. The reaction of HF with AlCl* and $Al(CH_3)$* surface species leads to a slight mass loss and can be expressed as AlCl* + $Al(CH_3)$* + 2HF → 2AlF* + HCl + CH_4. The fluorination of AlCl* to AlF* is thermochemically favorable. The reaction $AlCl_3$ + 3HF → AlF_3 + 3HCl has a standard free energy change of ΔG° = −61 kcal/mol at 250 °C.[30]

HF can also fluorinate the Al_2O_3 substrate and form an AlF_3 or AlF_xO_y surface layer.[28,29] The fluorination reaction leads to mass gain that is larger than the mass loss resulting from the reaction of HF with AlCH* and AlCl* species. The fluorination reaction Al_2O_3 + 6HF → 2AlF_3 + 3H_2O is spontaneous at 200−300 °C. The standard free energy changes are negative with values of ΔG°= −58.4 kcal/mol at 200 °C and ΔG° = −49.1 kcal/mol at 300 °C.[30]

Figure 6 also shows that the fluorination of Al_2O_3 to form an AlF_3 or AlF_xO_y surface layer is fairly constant at different temperatures. The comparable mass changes at different temperatures suggest a similar AlF_3 or AlF_xO_y layer thickness. Previous experiments of HF exposures on hydroxylated Al_2O_3 substrates also showed constant mass gains of ΔM_{HF} = 35−38 ng/cm^2 at 150−250 °C.[12]

After the creation of the AlF_3 or AlF_xO_y layer by HF, the next DMAC exposure removes the AlF_3 or AlF_xO_y layer by ligand exchange as demonstrated by the mass losses shown in Figure 6. The DMAC and HF cycles show a mass loss in the second cycle for temperatures at 250−300 °C. The DMAC and HF cycles at 225 °C show a mass loss at the fourth ALE cycle. Figure 6 indicates that more removal of AlF_3 or AlF_xO_y by DMAC at higher temperatures results in a larger mass gain for the subsequent fluorination of Al_2O_3 by HF. Similar behavior was observed during Al_2O_3 ALE using TMA and HF exposures.[12]

Figure 7 shows the ΔM_{DMAC}, ΔM_{HF}, and MCPC values at 200−300 °C in the steady state etching region. The ΔM_{DMAC}, ΔM_{HF}, MCPC, and etch rate values are summarized in Table 1. The same reaction sequence of 2−30−1−30 was employed for all Al_2O_3 ALE reactions. ΔM_{DMAC} shows increasingly larger mass losses at higher temperatures. In contrast, ΔM_{HF} shows

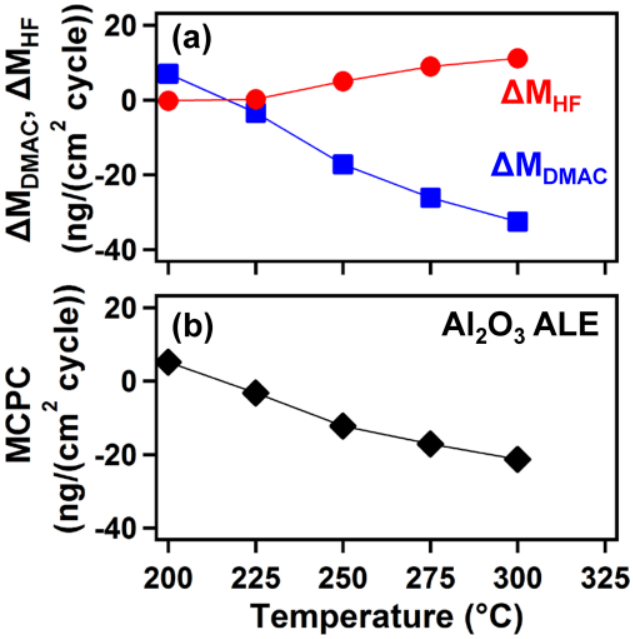

Figure 7. Temperature dependence of (a) ΔM_{DMAC} and ΔM_{HF} and (b) MCPC for Al_2O_3 ALE.

increasingly larger mass gains at higher temperatures. Figure 7b reveals that the temperature dependence of MCPC follows the temperature dependence of ΔM_{DMAC}. More removal of AlF_3 or AlF_xO_y by DMAC exposure leads to the higher etch rate of Al_2O_3 at higher temperature. Higher ΔM_{HF} at higher temperature compensates for the removal of AlF_3 or AlF_xO_y to maintain a nearly constant AlF_3 or AlF_xO_y thickness.

III.B. *Ex Situ* XRR and SE Measurements for Thermal Al_2O_3 ALE. Al_2O_3 ALE was also studied using *ex situ* XRR and SE measurements. Al_2O_3 ALD films were grown on Si(100) wafers using 150 cycles of TMA and H_2O at 250 °C with a reaction sequence of 1−20−1−20. Figure 8a shows the film thicknesses of the initial Al_2O_3 film and the Al_2O_3 film after 10, 25, 50, 100, and 200 ALE cycles at 250 °C. The accuracy of these film thickness measurements is ±0.5 Å. The initial Al_2O_3 ALD films grown at 250 °C have a thickness of 151 Å. The film thickness is then reduced linearly versus number of ALE cycles with an etch rate of 0.31 Å/cycle. The spectroscopic ellipsometry (SE) measurements on these same Al_2O_3 films also yield an etch rate of 0.31 Å/cycle. The etch rates determined by XRR and SE are comparable to the etch rate of 0.39 Å/cycle obtained by the *in situ* QCM experiments at 250 °C.

Figure 8b shows the root-mean-square (RMS) roughness of the Al_2O_3 ALD films obtained from the XRR analysis. The accuracy of these surface roughness measurements is ±0.3 Å. The initial Al_2O_3 ALD film has a roughness of ∼5 Å. The Al_2O_3 films become smoother versus Al_2O_3 ALE cycles. The surface roughness reduced to ∼2.5 Å after 10 ALE cycles. The surface roughness then reduces further to ∼1.5 Å after 100−200 ALE cycles. The uncertainty in these XRR surface roughness measurements is ±0.5 Å. Similar surface smoothening versus number of ALE cycles has been observed during Al_2O_3 ALE using HF and $Sn(acac)_2$,[6] Al_2O_3 ALE using HF and TMA,[31] ZnO ALE using HF and TMA,[32] and HfO_2 ALE using HF and $Sn(acac)_2$.[10]

DOI: 10.1021/acs.jpcc.9b04767
J. Phys. Chem. C 2019, 123, 18455−18466

Table 1. MCPC, Etch Rate, ΔM_{DMAC}, and ΔM_{HF} for Thermal Al_2O_3, HfO_2, and ZrO_2 ALE at Different Temperatures[a]

material	temperature (°C)	MCPC ng/(cm^2 cycle)	etch rate (Å/cycle)	ΔM_{DMAC} ng/(cm^2 cycle)	ΔM_{HF} ng/(cm^2 cycle)
Al_2O_3	225	−3.2	0.10	−3.4	0.2
Al_2O_3	250	−12.2	0.39	−17.2	5.0
Al_2O_3	275	−17.1	0.55	−26.1	9.0
Al_2O_3	300	−21.3	0.69	−32.5	11.2
HfO_2	200	−34.6	0.36	−28.5	−6.1
HfO_2	225	−76.0	0.79	−72.8	−3.2
HfO_2	250	−94.1	0.98	−93.6	−0.5
HfO_2	275	−105.4	1.10	−107.0	1.7
HfO_2	300	−118.8	1.24	−120.6	1.8
ZrO_2	200	−52.1	0.91	−50.8	−1.3
ZrO_2	225	−67.5	1.18	−69.1	1.6
ZrO_2	250	−75.6	1.33	−79.1	3.4
ZrO_2	275	−85.8	1.51	−95.0	9.3
ZrO_2	300	−90.5	1.59	−103.3	12.8

[a]Accuracy of MCPC, ΔM_{DMAC}, and ΔM_{HF} is ±0.3 ng/(cm^2 cycle).

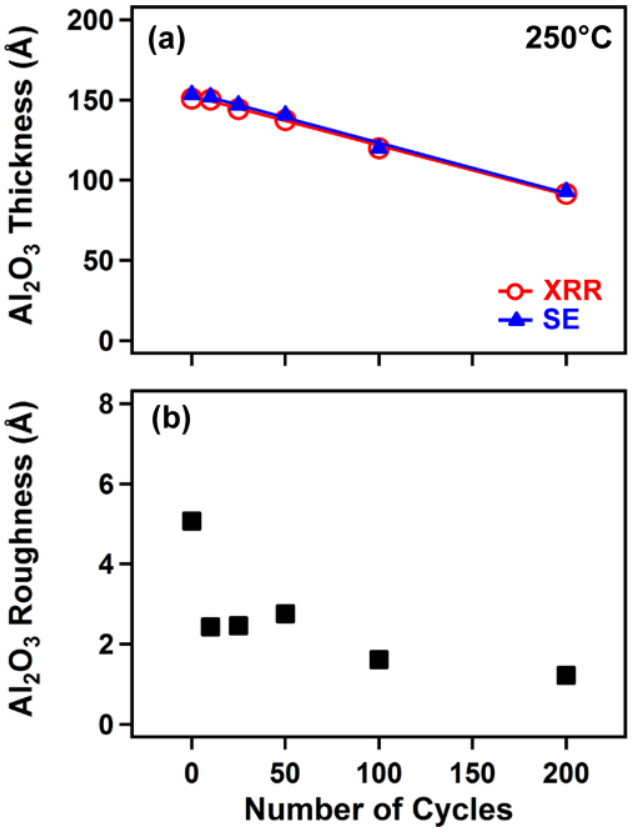

Figure 8. (a) X-ray reflectivity and spectroscopic ellipsometry measurements of Al_2O_3 film thickness versus number of Al_2O_3 ALE cycles. (b) Al_2O_3 film roughness versus number of Al_2O_3 ALE cycles for initial Al_2O_3 ALD films.

III.C. Proposed Mechanism of Thermal Al_2O_3 ALE.

Figure 9 illustrates the proposed reaction mechanism for thermal Al_2O_3 ALE using sequential HF and DMAC exposures. This mechanism is based on the mass changes during the HF and DMAC exposures as observed by the QCM measurements. During the fluorination reaction (A), HF reacts with $AlCH_3$* and AlCl* surface species to form AlF* surface species and CH_4 and HCl reaction products. HF also fluorinates the underlying Al_2O_3 film to form an AlF_3 or AlF_xO_y surface layer and H_2O reaction products.

During the ligand-exchange reaction (B), DMAC removes the AlF_3 or AlF_xO_y surface layer on the Al_2O_3 substrate and is expected to form volatile $AlF(CH_3)_2$ and $AlFCl(CH_3)$ reaction products. Mass spectrometry studies are needed to confirm these etch products. DMAC and one of the possible etch products, $AlF(CH_3)_2{\cdot}AlFClCH_3$, are shown as dimers. $AlF(CH_3)_2$ has a vapor pressure of 80 Torr at 100 °C.[33] $AlFCl(CH_3)$ is expected to be volatile. $AlCl(CH_3)_2$ may also react with the underlying Al_2O_3 substrate to form AlCl* and $Al(CH_3)$* after the elimination of AlF* species.

The simplest overall reaction assuming CH_3 ligand transfer during the ligand-exchange reaction can be written as

$$Al_2O_3 + 6HF + 4AlCl(CH_3)_2 \rightarrow 2AlF(CH_3)_2 + 4AlFCl(CH_3) + 3H_2O \quad (1)$$

This overall reaction can be split into the HF and DMAC reactions:

$$(A)\ Al_2O_3|Al_2O_3^{\ddagger} + 6HF \rightarrow Al_2O_3|2AlF_3^{\ddagger} + 3H_2O \quad (2)$$

$$(B)\ Al_2O_3|2AlF_3^{\ddagger} + 4AlCl(CH_3)_2 \rightarrow Al_2O_3^{\ddagger} + 2AlF(CH_3)_2 + 4AlFCl(CH_3) \quad (3)$$

The amount of Al_2O_3 that is etched during the ALE reaction cycle is given by $Al_2O_3^{\ddagger}$ in eqs 2 and 3. The vertical lines are meant to separate the surface species. $2AlF_3^{\ddagger}$ is the amount of AlF_3 corresponding with the amount of Al_2O_3 that is etched during the ALE reaction cycle.

The reactions described by eqs 1−3 may be incomplete because DMAC may also interact with the etched surface. The reaction of DMAC with Al_2O_3 could form both $AlCH_3$* and AlCl* surface species. DMAC may also interact with AlF_3 surface species remaining due to incomplete etching. This interaction may lead to F/Cl exchange.

In comparison to this thermal Al_2O_3 ALE process, plasma Al_2O_3 ALE has also been demonstrated using sequential exposures of BCl_3 gas to chlorinate the Al_2O_3 surface and bombardment by energetic neutral Ar beams to remove the surface chloride species.[34] The Ar beams were formed by

DOI: 10.1021/acs.jpcc.9b04767
J. Phys. Chem. C 2019, 123, 18455−18466

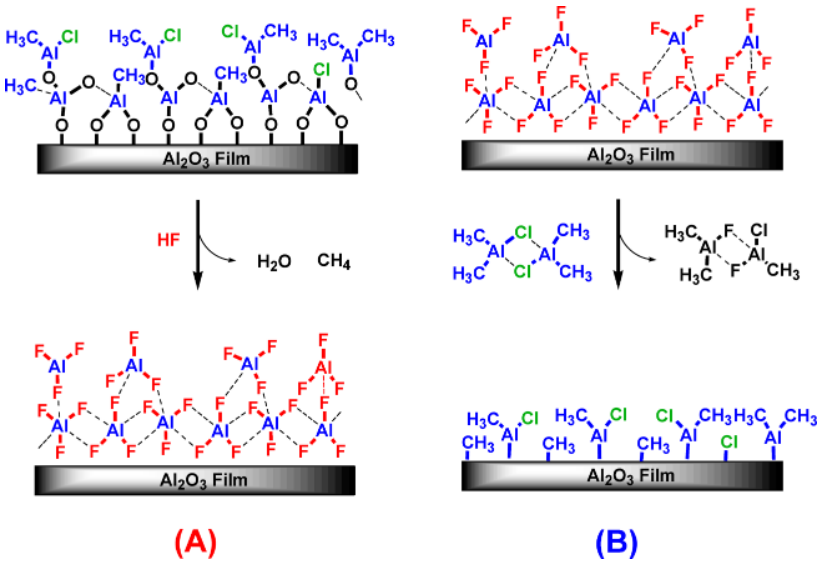

Figure 9. Schematic of proposed reaction mechanism for thermal Al_2O_3 ALE showing (A) HF reaction and (B) DMAC reaction.

neutralizing Ar^+ ion beams from an inductively coupled plasma ion gun. Al_2O_3 etch rates of ~1 Å/cycle were obtained using a grid voltage of 100 V for the Ar^+ ion beam.[34]

III.D. *In Situ* QCM Measurements for Thermal ALE of HfO_2 and ZrO_2. HfO_2 and ZrO_2 ALE were also studied by QCM measurements using sequential DMAC and HF exposures at 200–300 °C. The initial HfO_2 ALD films on the QCM sensor were grown using TDMAH and H_2O as the reactants.[26] The initial ZrO_2 ALD films were grown using TEMAZ and H_2O as the reactants.[26] The reaction sequence for the HfO_2 and ZrO_2 ALD was 1–40–1–40. Figure 10 shows the mass change during 100 cycles of HfO_2 and ZrO_2 ALE at 250 °C using the DMAC and HF reaction sequence of 2–30–1–30.

Figure 10a and 10b reveal that the mass changes are linear versus the number of sequential DMAC and HF exposures. The mass changes versus number of reaction cycles in Figure 10a and 10b yield MCPC = −94.1 ng/(cm^2 cycle) for HfO_2 ALE and MCPC = −75.6 ng/(cm^2 cycle) for ZrO_2 ALE, respectively. These MCPCs are consistent with etch rates of 0.98 Å/cycle for HfO_2 ALE and 1.33 Å/cycle for ZrO_2 ALE.

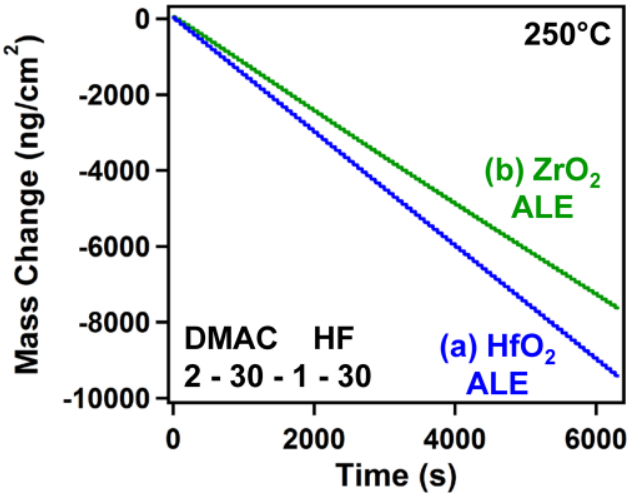

Figure 10. Mass change versus time during 100 cycles of: (a) HfO_2 ALE and (b) ZrO_2 ALE at 250 °C using the reaction sequence of 2–30–1–30.

Figure 11 displays the mass changes during three sequential cycles of HfO_2 and ZrO_2 ALE at 250 °C. These three cycles are from enlargements of the linear etching regions of HfO_2 and ZrO_2 ALE shown in Figure 10. Figure 11a shows the mass changes coinciding with the DMAC and HF exposures for HfO_2 ALE. The mass loss during the DMAC exposure for 2.0 s is very prompt with little additional change during the purge time. A mass change of ΔM_{DMAC} = −93.6 ng/(cm^2 cycle) was observed after the DMAC exposure. This mass decrease is consistent with the removal of the HfF_4 surface layer on the HfO_2 substrate. DMAC is able to transfer either Cl or CH_3 ligands. The ligand exchange of Cl from DMAC to HfF_4 to form $HfCl_4$ or $HfCl_xF_{4-x}$ mixed halogen species is most likely. $HfCl_4$ is stable and volatile at 250 °C. The vapor pressure of $HfCl_4$ is 1 Torr at 190 °C.[18] $Hf(CH_3)_4$ may be volatile but has limited stability at high temperature.[7,35] Very little is known about $HfCl_xF_{4-x}$ mixed halogen species.

The mass change after the HF exposure for 1.0 s is very small at ΔM_{HF} = −0.5 ng/(cm^2 cycle). In contrast, the fluorination of HfO_2 to HfF_4 by HF should produce a mass increase. The molar masses of HfO_2 and HfF_4 are 210.5 g/mol and 254.5 g/mol, respectively. The negligible mass change for ΔM_{HF} suggests that the concurrent fluorination of the HfCl* species by HF to form a HfF* species must produce a mass loss. The balance of the mass gain and loss during fluorination then would result in a small mass change.

Figure 11b shows the mass changes during the DMAC and HF exposures for ZrO_2 ALE. The mass loss during the DMAC exposure for 2.0 s is again very rapid. A mass change of ΔM_{DMAC} = −79.1 ng/(cm^2 cycle) was observed after the DMAC exposure. This mass decrease is consistent with the removal of the ZrF_4 surface layer on the ZrO_2 substrate. In comparison, previous studies revealed that TMA and HF exposures could not etch ZrO_2.[7] These results were explained by the instability of $Zr(CH_3)_4$ at high temperature.[7,36] In contrast, DMAC can transfer Cl ligands and form $ZrCl_4$ or $ZrCl_xF_{4-x}$ mixed halogen species. $ZrCl_4$ is stable and volatile at 250 °C. The vapor pressure of $ZrCl_4$ is 1 Torr at 190 °C.[18]

DOI: 10.1021/acs.jpcc.9b04767
J. Phys. Chem. C 2019, 123, 18455−18466

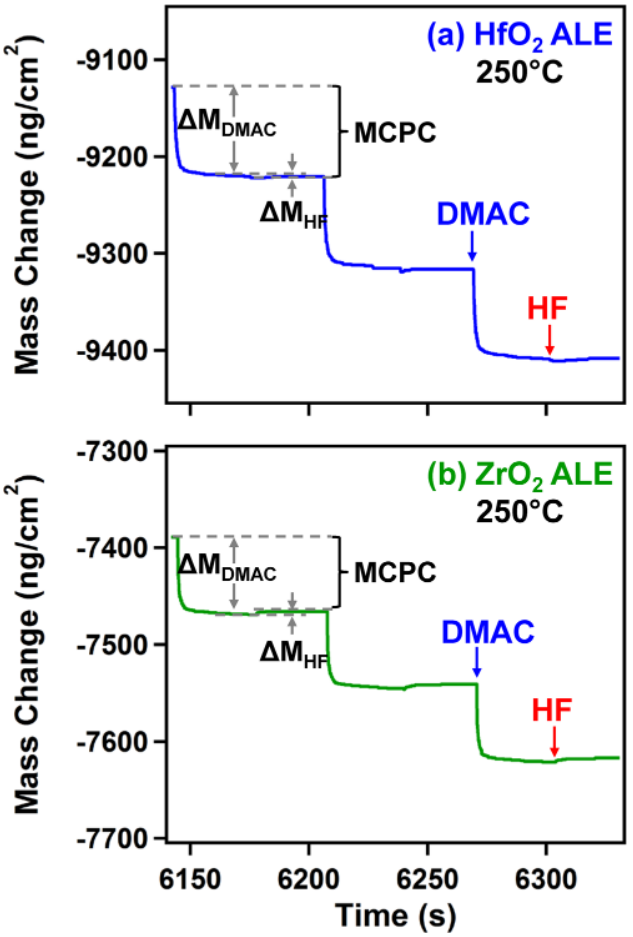

Figure 11. Enlargement of mass change versus time in Figure 10 for three sequential DMAC and HF exposures in the steady state, linear etching region at 250 °C during: (a) HfO_2 ALE and (b) ZrO_2 ALE.

Almost nothing has been reported about $ZrCl_xF_{4-x}$ mixed halogen species.

The mass change after the HF exposure for 1.0 s is small at ΔM_{HF} = +3.4 ng/(cm^2 cycle). The fluorination of ZrO_2 to ZrF_4 should produce a mass gain. The molar masses of ZrO_2 and ZrF_4 are 123.2 g/mol and 167.2 g/mol, respectively. The small mass change argues that the simultaneous reaction of HF with ZrCl* species to form ZrF* species must produce a mass loss. The balance between mass gain and mass loss leads to a small mass increase.

Both HfO_2 and ZrO_2 ALE reactions displayed self-limiting reactions. The self-limiting behavior was examined by monitoring mass changes versus exposure for each reactant. ΔM_{DMAC}, ΔM_{HF}, MCPC, and the etch rate for HfO_2 and ZrO_2 ALE at the different temperatures are summarized in Table 1. Etch rates for HfO_2 and ZrO_2 ALE were calculated using the MCPCs and the XRR densities of 9.6 g/cm^3 for HfO_2 ALD film and 5.7 g/cm^3 for ZrO_2 ALD film, respectively.

III.E. Proposed Mechanism of Thermal HfO_2 and ZrO_2 ALE. Figure 12 shows the proposed reaction mechanism for thermal MO_2 (M = Hf or Zr) ALE. This mechanism is based on the mass changes during the HF and DMAC exposures as obtained by the QCM measurements. During the fluorination reaction (A), HF reacts with MCl* surface species to form MF* surface species and HCl reaction products. HF also reacts with the underlying MO_2 film to form an MF_4 surface layer and

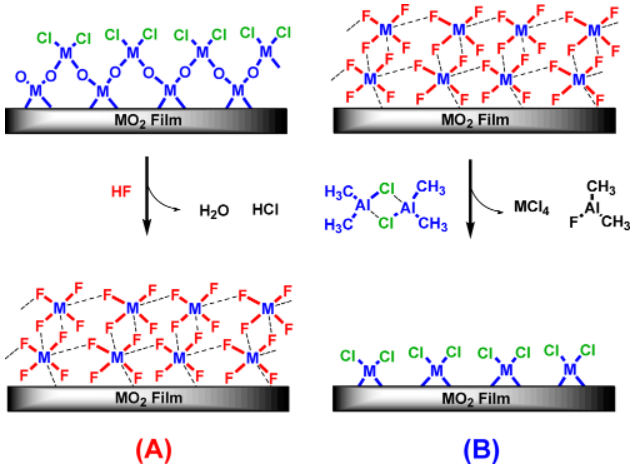

Figure 12. Schematic of proposed reaction mechanism for thermal MO_2 (M = Hf or Zr) ALE showing (A) HF reaction and (B) DMAC reaction.

H_2O reaction products. During the ligand-exchange reaction (B), DMAC reacts with the MF_4 surface layer on the MO_2 substrate to form volatile MCl_4 or MCl_xF_{4-x} mixed halogen species and $AlF(CH_3)_2$ reaction products.

$HfCl_4$ and $ZrCl_4$ are volatile solids having sublimation temperatures of 317 and 331 °C, respectively.[18] Vapor pressures of $HfCl_4$ and $ZrCl_4$ are 1 Torr at 190 °C.[18] Mixed fluoride/chloride species such as $MFCl_3$ or MF_2Cl_2 may also be etch products if they have a high enough vapor pressure. The etch products with M−CH_3 bonds such as $MF_xCl_y(CH_3)_{4-x-y}$ or $MF_x(CH_3)_{4-x}$ may be possible, but the M−Cl bond is much more stable than the M−CH_3 bond. Figure 12 includes only MCl* surface species because of the higher stability of the M−Cl bond compared with the M−CH_3 bond. Chemical equations could also be written for the surface chemical reactions that are similar to eqs 2 and 3.

Plasma HfO_2 and ZrO_2 ALE have also been performed using sequential exposures of BCl_3 gas to chlorinate the HfO_2 and ZrO_2 surfaces and bombardment by energetic neutral Ar beams to desorb the surface chloride species.[37,38] The Ar beams were formed by neutralizing Ar^+ ion beams. HfO_2 and ZrO_2 etch rates of ∼1 Å/cycle were obtained using the sequential BCl_3 and energetic neutral Ar beam exposures.[37,38]

III.F. Etch Rates and Fluoride Thicknesses for Thermal Al_2O_3, HfO_2, and ZrO_2 ALE. Figure 13 shows the etch rates for thermal Al_2O_3, HfO_2, and ZrO_2 ALE using DMAC and HF at different temperatures. These etch rates were determined from the MCPCs measured by *in situ* QCM studies using the density of the metal oxides to convert between mass and thickness. The etch rates increase versus temperature from 200 to 300 °C. The relative etch rates also vary with the metal oxides according to ZrO_2 > HfO_2 > Al_2O_3. The etch rates for Al_2O_3 ALE increased from 0.10 Å/cycle to 0.69 Å/cycle at temperatures from 225 to 300 °C. The etch rates for HfO_2 ALE increased from 0.36 Å/cycle to 1.24 Å/cycle at temperatures from 200 to 300 °C. The etch rates for ZrO_2 ALE increased from 0.91 Å/cycle to 1.59 Å/cycle at temperatures from 200 to 300 °C.

The thicknesses of the metal fluorides on Al_2O_3, HfO_2, and ZrO_2 during thermal ALE are also consistent with the relative etch rates. In the previous study of Al_2O_3 ALE,[12] the mass gain of 34 ng/cm^2 after HF exposures on fresh Al_2O_3 ALD surfaces

DOI: 10.1021/acs.jpcc.9b04767
J. Phys. Chem. C 2019, 123, 18455−18466

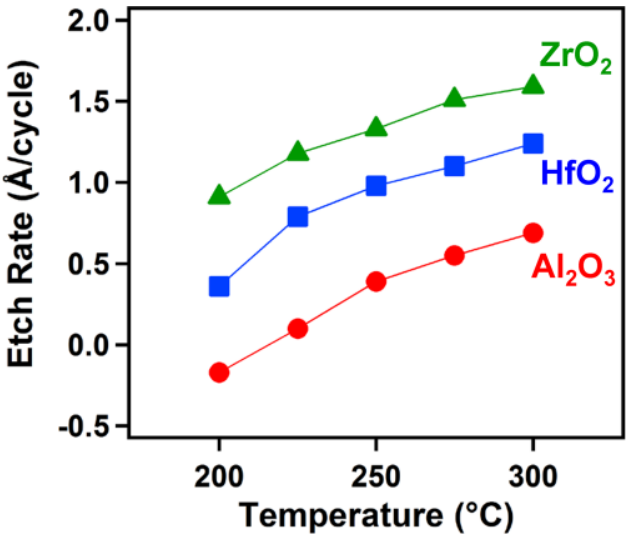

Figure 13. Etch rates for Al_2O_3, HfO_2, and ZrO_2 ALE at different temperatures using DMAC and HF.

was employed to calculate the thickness of the AlF_3 layer. These calculations revealed that 1.7 Å of Al_2O_3 was converted to an AlF_3 layer with a thickness of 3.0 Å during thermal Al_2O_3 ALE.[12]

In comparison, HF exposures on initial HfO_2 substrates showed mass gains of ΔM_{HF} = 36−41 ng/cm^2 at 150−300 °C. The fluorination reaction $HfO_2 + 4HF \rightarrow HfF_4 + 2H_2O$ will result in a mass increase of 12% from 210.5 amu for HfO_2 to 254.5 amu for HfF_4. The average value of ΔM_{HF} = 39 ng/cm^2 corresponds to the conversion of 186.6 ng/cm^2 of HfO_2 to 225.6 ng/cm^2 of the HfF_4 layer. Based on the density of 9.6 g/cm^3 for HfO_2, the mass of 186.6 ng/cm^2 for HfO_2 is equivalent to a HfO_2 thickness of 1.9 Å. Similarly, based on the density of 6.8 g/cm^3 for HfF_4,[27] the mass of 225.6 ng/cm^2 for HfF_4 is equivalent to a HfF_4 thickness of 3.3 Å.

HF exposures on initial ZrO_2 substrates displayed mass gains of ΔM_{HF} = 45−50 ng/cm^2 at 200−300 °C. The fluorination reaction $ZrO_2 + 4HF \rightarrow ZrF_4 + 2H_2O$ will result in a mass increase of 36% from 123.2 amu for ZrO_2 to 167.2 amu for ZrF_4. The average value of ΔM_{HF} = 48 ng/cm^2 corresponds to the conversion of 134.4 ng/cm^2 of ZrO_2 to 182.4 ng/cm^2 of the ZrF_4 layer. Based on the density of 5.7 g/cm^3 for ZrO_2, the mass of 134.4 ng/cm^2 for ZrO_2 is equivalent to a ZrO_2 thickness of 2.4 Å. Similarly, based on the density of 4.1 g/cm^3 for ZrF_4,[27] the mass of 182.4 ng/cm^2 for ZrF_4 is equivalent to a ZrF_4 thickness of 4.4 Å.

The values for the fluoride thicknesses are in the same relative order as the values for the etch rates at 250 °C. The fluoride thicknesses are 3.0, 3.3, and 4.4 Å for Al_2O_3, HfO_2, and ZrO_2, respectively. The etch rates are 0.39, 0.98, and 1.33 Å/cycle at 250 °C for Al_2O_3, HfO_2, and ZrO, respectively. The correlation between the fluoride thicknesses and the etch rates was also observed for Al_2O_3 ALE versus HF pressure.[28] Higher HF pressures led to thicker AlF_3 film thicknesses and higher Al_2O_3 etch rates.[28]

III.G. Comparison between DMAC and TMA for Thermal Al_2O_3, HfO_2, and ZrO_2 ALE. Figure 14 compares DMAC and TMA for thermal Al_2O_3, HfO_2, and ZrO_2 ALE at 250 °C. Figure 14a shows the comparison of the mass changes versus time during four sequential cycles using either DMAC or TMA together with HF for Al_2O_3 ALE. Following the initial

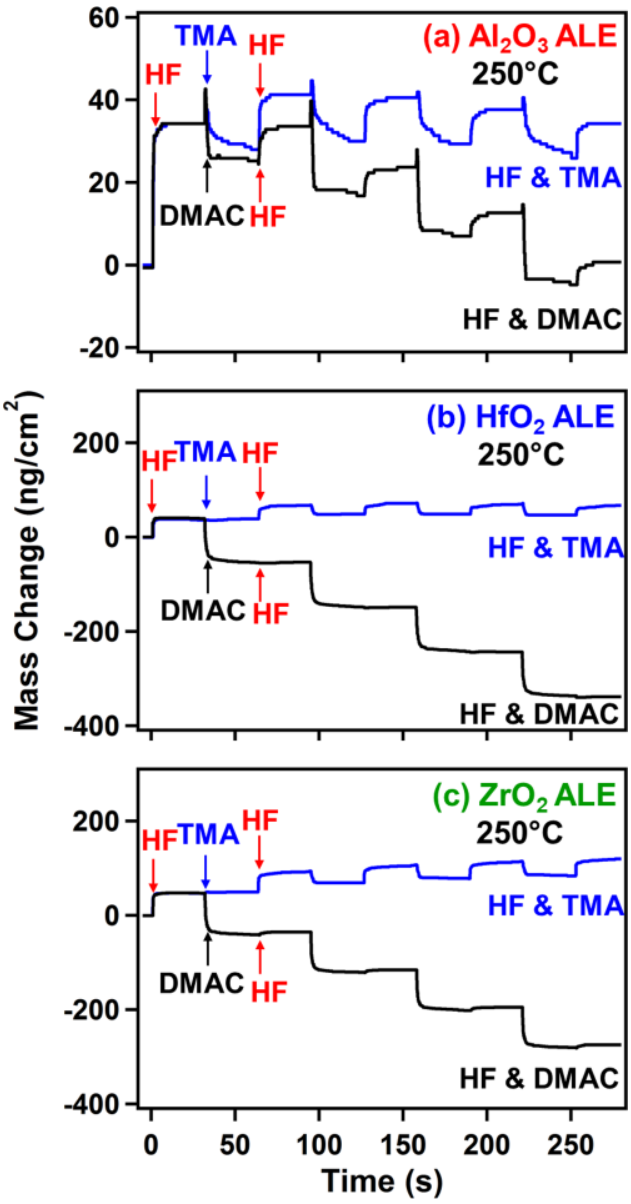

Figure 14. Comparison of mass changes versus time during four sequential exposures of HF and TMA or HF and DMAC on: (a) Al_2O_3; (b) HfO_2; and (c) ZrO_2 at 250 °C using the reaction sequence of 2−30−1−30.

nucleation, sequential HF and TMA exposures etch the Al_2O_3 film with an etch rate of −4.2 ng/cm^2. In contrast, sequential HF and DMAC exposures etch the Al_2O_3 film at a much faster etch rate of −12.2 ng/cm^2. The larger etch rate for DMAC is attributed to the Cl ligand on DMAC. The Cl ligand yields a more efficient ligand-exchange reaction. The individual mass changes for DMAC and TMA measured by the QCM are also consistent with Cl present on the surface after the DMAC exposure during Al_2O_3 ALE.

Figure 14b shows the comparison of the mass changes versus time during four sequential cycles using either DMAC or TMA together with HF exposures for HfO_2 ALE. The QCM results reveal that sequential HF and TMA exposures lead to negligible HfO_2 etching in agreement with previous studies.[7] In contrast, sequential HF and DMAC exposures etch the HfO_2 film with a mass loss of −94.1 ng/cm^2 or 0.98 Å/

DOI: 10.1021/acs.jpcc.9b04767
J. Phys. Chem. C 2019, 123, 18455−18466

cycle. This selectivity results from the ability of DMAC to provide a Cl ligand during ligand exchange. As discussed earlier, Hf–Cl bonds are stable, and $HfCl_4$ is volatile. Hf–C bonds are also weaker, and $Hf(CH_3)_4$ is unstable at higher temperatures.

Figure 14c shows the comparison of the mass changes versus time during four sequential cycles using either DMAC or TMA together with HF for ZrO_2 ALE. Similar to the comparison in Figure 14b, HF and TMA do not etch ZrO_2 in agreement with previous results.[7] In contrast, sequential HF and DMAC exposures etch the ZrO_2 film with a mass loss per cycle of MCPC = −75.6 ng/cm^2 or 1.33 Å/cycle. This selectivity again results from the ability of DMAC to transfer a Cl ligand during the ligand-exchange reaction. Zr–Cl bonds are stable, and $ZrCl_4$ is volatile as mentioned earlier. Zr–C bonds are also weaker, and $Zr(CH_3)_4$ is unstable at higher temperatures.

III.H. Etching of Masked Al_2O_3 Substrates. The selectivity of thermal Al_2O_3 ALE was also demonstrated by using sequential exposures of HF and DMAC to etch a masked Al_2O_3 substrate. The mask was SiN; the etched material was Al_2O_3; and the etch stop was SiO_2. Figure 15a shows a schematic of the test structure used to demonstrate selective etching by thermal Al_2O_3 ALE. Because thermal ALE is isotropic, the Al_2O_3 film underlying the SiN mask should be etched resulting from the nondirectional nature of thermal ALE. This undercutting is illustrated in Figure 15a.

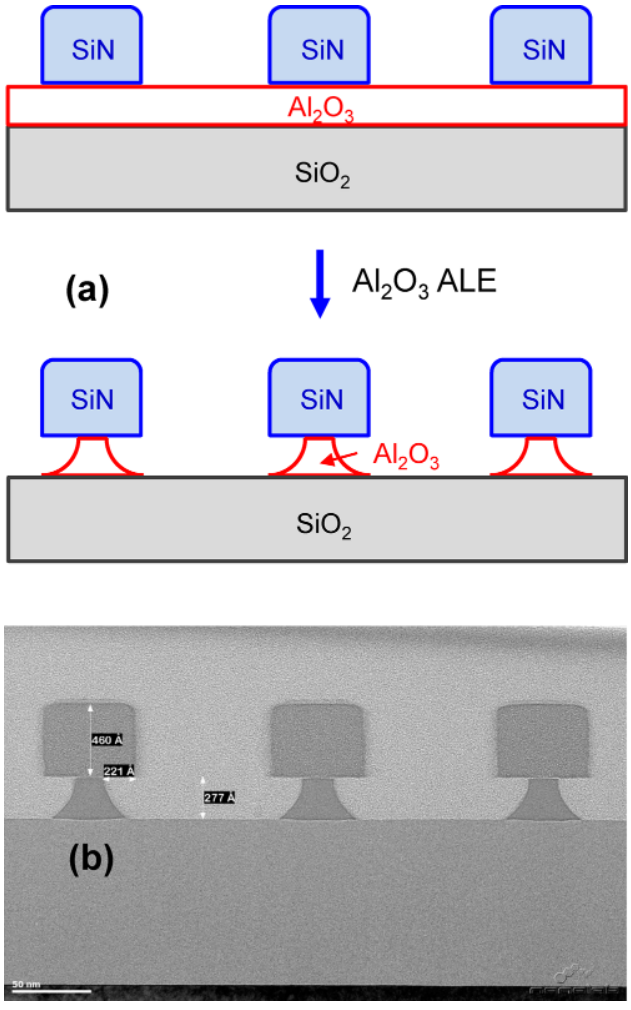

Figure 15. (a) Schematic for isotropic etching of Al_2O_3 using masked substrate. (b) TEM image of masked substrate after 1000 cycles of Al_2O_3 ALE using HF and DMAC at 250 °C with the reaction sequence of 2–30–1–30.

Figure 15b reveals the transmission electron microscopy (TEM) image of the masked substrate after 1000 cycles of Al_2O_3 ALE using HF and DMAC at 250 °C. The initial structure consists of a plasma-enhanced chemical vapor deposition (PECVD) SiN patterned mask with a thickness of 46 nm on an Al_2O_3 film with a thickness of 28 nm on a thermal SiO_2 film. The Al_2O_3 film not covered by the SiN mask is etched by thermal Al_2O_3 ALE. There is undercut etching of Al_2O_3 beneath the SiN mask because thermal ALE is isotropic. The thermal Al_2O_3 ALE is selective and does not etch the SiN or SiO_2 films in agreement with previous results.[7]

The Al_2O_3 ALE is reasonably isotropic. The 1000 cycles of Al_2O_3 ALE remove a 277 Å vertical thickness of Al_2O_3 in the unmasked region. The length of the horizontal lateral etch depth undercutting the SiN mask is 221 Å. The etching is not perfectly isotropic. The difference between the 277 Å vertical and 221 Å horizontal etch lengths may be dependent on gas conductance. The precursor exposures may not be self-limiting in the shadowed volumes underneath the SiN mask.

IV. CONCLUSIONS

The thermal ALE of Al_2O_3, HfO_2, and ZrO_2 was demonstrated using sequential exposures of HF and DMAC. DMAC is an effective metal reactant for thermal ALE using fluorination and ligand-exchange reactions because either CH_3 or Cl ligands can be transferred in the ligand-exchange reactions. Al_2O_3, HfO_2, and ZrO_2 ALE were studied at temperatures from 200 to 300 °C using QCM experiments. These QCM studies revealed that the mass loss during Al_2O_3, HfO_2, and ZrO_2 ALE was linear versus number of HF and DMAC exposures. In contrast, ZrO_2 and HfO_2 ALE were negligible using HF and TMA exposures. TMA only has CH_3 ligands that can transfer in the ligand-exchange reaction, and $Zr(CH_3)_4$ and $Hf(CH_3)_4$ etch products are not stable.

The etch rates for Al_2O_3, HfO_2, and ZrO_2 ALE using HF and DMAC were larger at higher temperatures. At 250 °C, the mass change per cycle of MCPC = −12.2, −93.6, and −79.1 ng/(cm^2 cycle) or etch rates of 0.39, 0.98, and 1.33 Å/cycle were measured for Al_2O_3, HfO_2, and ZrO_2 ALE using HF and DMAC. In comparison, the AlF_3, HfF_4, and ZrF_4 surface layers after the HF exposure were estimated to have a thickness of 3.0 Å, 3.3 Å, and 4.4 Å on Al_2O_3, HfO_2, and ZrO_2, respectively. The magnitudes of these fluoride thicknesses have the same ordering as the etch rates for Al_2O_3, HfO_2, and ZrO_2 ALE, respectively. A similar correlation between fluoride thickness and etch rate was observed recently during studies of the effect of HF pressure on Al_2O_3 ALE using HF and TMA.

XRR and SE studies confirmed the linear etching and the etch rates using HF and DMAC. XRR analysis also revealed the smoothening of the etched Al_2O_3 film. A comparison of Al_2O_3, HfO_2, and ZrO_2 ALE using either HF and DMAC or HF and TMA demonstrated that higher etch rates were observed with DMAC for all three materials. The etching of masked Al_2O_3 substrates also showed that Al_2O_3 ALE was reasonably isotropic and selective to Al_2O_3 in the presence of the SiN mask and SiO_2 etch stop. The ability of DMAC to provide either CH_3 or Cl ligands during the ligand-exchange reaction should be useful for the thermal ALE of a variety of materials.

DOI: 10.1021/acs.jpcc.9b04767
J. Phys. Chem. C 2019, 123, 18455−18466

AUTHOR INFORMATION

Corresponding Author

*E-mail: steven.george@colorado.edu.

ORCID

Younghee Lee: 0000-0002-0492-6826

Steven M. George: 0000-0003-0253-9184

Notes

The authors declare no competing financial interest.

ACKNOWLEDGMENTS

This research was funded by Intel Corporation through a Member Specific Research Project administered by the Semiconductor Research Corporation. Additional funding was obtained from the National Science Foundation (CHE-1609554). The authors thank Andreas Fischer and Thorsten Lill of Lam Research for the masked Al_2O_3 substrates and for TEM imaging of these substrates after thermal Al_2O_3 ALE.

REFERENCES

(1) Kanarik, K. J.; Lill, T.; Hudson, E. A.; Sriraman, S.; Tan, S.; Marks, J.; Vahedi, V.; Gottscho, R. A. Overview of Atomic Layer Etching in the Semiconductor Industry. *J. Vac. Sci. Technol., A* **2015**, *33*, No. 020802.

(2) Carver, C. T.; Plombon, J. J.; Romero, P. E.; Suri, S.; Tronic, T. A.; Turkot, R. B. Atomic Layer Etching: An Industry Perspective. *ECS J. Solid State Sci. Technol.* **2015**, *4*, N5005−N5009.

(3) Matsuura, T.; Murota, J.; Sawada, Y.; Ohmi, T. Self-Limited Layer-by-Layer Etching of Si by Alternated Chlorine Adsorption and Ar^+ Ion Irradiation. *Appl. Phys. Lett.* **1993**, *63*, 2803−2805.

(4) Sakaue, H.; Iseda, S.; Asami, K.; Yamamoto, J.; Hirose, M.; Horiike, Y. Atomic Layer Controlled Digital Etching of Silicon. *Jpn. J. Appl. Phys. 1* **1990**, *29*, 2648−2652.

(5) George, S. M.; Lee, Y. Prospects for Thermal Atomic Layer Etching Using Sequential, Self-Limiting Fluorination and Ligand-Exchange Reactions. *ACS Nano* **2016**, *10*, 4889−4894.

(6) Lee, Y.; George, S. M. Atomic Layer Etching of Al_2O_3 Using Sequential, Self-Limiting Thermal Reactions with $Sn(acac)_2$ and HF. *ACS Nano* **2015**, *9*, 2061−2070.

(7) Lee, Y.; Huffman, C.; George, S. M. Selectivity in Thermal Atomic Layer Etching Using Sequential, Self-Limiting Fluorination and Ligand-Exchange Reactions. *Chem. Mater.* **2016**, *28*, 7657−7665.

(8) Lee, Y.; DuMont, J. W.; George, S. M. Mechanism of Thermal Al_2O_3 Atomic Layer Etching Using Sequential Reactions with $Sn(acac)_2$ and HF. *Chem. Mater.* **2015**, *27*, 3648−3657.

(9) Johnson, N. R.; Sun, H. X.; Sharma, K.; George, S. M. Thermal Atomic Layer Etching of Crystalline Aluminum Nitride Using Sequential, Self-limiting Hydrogen Fluoride and $Sn(acac)_2$ Reactions and Enhancement by H_2 and Ar Plasmas. *J. Vac. Sci. Technol., A* **2016**, *34*, No. 050603.

(10) Lee, Y.; DuMont, J. W.; George, S. M. Atomic Layer Etching of HfO_2 Using Sequential, Self-Limiting Thermal Reactions with $Sn(acac)_2$ and HF. *ECS J. Solid State Sci. Technol.* **2015**, *4*, N5013−N5022.

(11) Lee, Y.; DuMont, J. W.; George, S. M. Atomic Layer Etching of AlF_3 Using Sequential, Self-Limiting Thermal Reactions with $Sn(acac)_2$ and Hydrogen Fluoride. *J. Phys. Chem. C* **2015**, *119*, 25385−25393.

(12) Lee, Y.; DuMont, J. W.; George, S. M. Trimethylaluminum as the Metal Precursor for the Atomic Layer Etching of Al_2O_3 Using Sequential, Self-Limiting Thermal Reactions. *Chem. Mater.* **2016**, *28*, 2994−3003.

(13) Hennessy, J.; Moore, C. S.; Balasubramanian, K.; Jewell, A. D.; France, K.; Nikzad, S. Enhanced Atomic Layer Etching of Native Aluminum Oxide for Ultraviolet Optical Applications. *J. Vac. Sci. Technol., A* **2017**, *35*, No. 041512.

(14) Lee, Y.; George, S. M. Thermal Atomic Layer Etching of HfO_2 Using HF for Fluorination and $TiCl_4$ for Ligand-Exchange. *J. Vac. Sci. Technol., A* **2018**, *36*, No. 061504.

(15) Roesky, H. W.; Haiduc, I. Fluorine as a Structure-directing Element in Organometallic Fluorides: Discrete Molecules, Supramolecular Self-Assembly and Host-guest Complexation. *J. Chem. Soc., Dalton Trans.* **1999**, 2249−2264.

(16) George, S. M. Atomic Layer Deposition: An Overview. *Chem. Rev.* **2010**, *110*, 111−131.

(17) Puurunen, R. L. Surface Chemistry of Atomic Layer Deposition: A Case Study for the Trimethylaluminum/water Process. *J. Appl. Phys.* **2005**, *97*, 121301.

(18) *CRC Handbook of Chemistry and Physics*; CRC PressOhio: Cleveland, 2018.

(19) Laubengayer, A. W.; Gilliam, W. F. The Alkyls of the Third Group Elements. I. Vapor Phase Studies of the Alkyls of Aluminum, Gallium and Indium. *J. Am. Chem. Soc.* **1941**, *63*, 477−479.

(20) Brockway, L. O.; Davidson, N. R. The Molecular Structure of the Dimers of Aluminum Dimethyl Chloride, Aluminum Dimethyl Bromide, and Aluminum Trimethyl and of Hexamethyldisilane. *J. Am. Chem. Soc.* **1941**, *63*, 3287−3297.

(21) Tanaka, J.; Smith, S. R. Mass Spectra of Bridge-bonded Aluminum Compounds. *Inorg. Chem.* **1969**, *8*, 265.

(22) Davidson, N.; Brown, H. C. The Polymerization of Some Derivatives of Trimethylaluminum. *J. Am. Chem. Soc.* **1942**, *64*, 316−324.

(23) Almenningen, A.; Halvorsen, S.; Haaland, A. Molecular Structureof the Trimethylaluminum Monomer. *J. Chem. Soc. D* **1969**, *12*, 644.

(24) Elam, J. W.; Groner, M. D.; George, S. M. Viscous Flow Reactor with Quartz Crystal Microbalance for Thin Film Growth by Atomic Layer Deposition. *Rev. Sci. Instrum.* **2002**, *73*, 2981−2987.

(25) Lee, Y.; DuMont, J. W.; Cavanagh, A. S.; George, S. M. Atomic Layer Deposition of AlF_3 Using Trimethylaluminum and Hydrogen Fluoride. *J. Phys. Chem. C* **2015**, *119*, 14185−14194.

(26) Hausmann, D. M.; Kim, E.; Becker, J.; Gordon, R. G. Atomic Layer Deposition of Hafnium and Zirconium Oxides Using Metal Amide Precursors. *Chem. Mater.* **2002**, *14*, 4350−4358.

(27) Lee, Y.; Sun, H. X.; Young, M. J.; George, S. M. Atomic Layer Deposition of Metal Fluorides Using HF-Pyridine as the Fluorine Precursor. *Chem. Mater.* **2016**, *28*, 2022−2032.

(28) Cano, A. M.; Marquardt, A. E.; DuMont, J. W.; George, S. M. Effect of HF Pressure on Thermal Al_2O_3 Atomic Layer Etch Rates and Al_2O_3 Fluorination. *J. Phys. Chem. C* **2019**, *123*, 10346−10355.

(29) Kondati Natarajan, S.; Elliott, S. D. Modeling the Chemical Mechanism of the Thermal Atomic Layer Etch of Aluminum Oxide: A Density Functional Theory Study of Reactions during HF Exposure. *Chem. Mater.* **2018**, *30*, 5912−5922.

(30) HSC Chemistry, *HSC Chemistry 5.1*; Outokumpu Research Oy: Pori, Finland.

(31) Zywotko, D. R.; Faguet, J.; George, S. M. Rapid Atomic Layer Etching of Al_2O_3 Using Sequential Exposures of Hydrogen Fluoride and Trimethylaluminum with No Purging. *J. Vac. Sci. Technol., A* **2018**, *36*, No. 061508.

(32) Zywotko, D. R.; George, S. M. Thermal Atomic Layer Etching of ZnO by a "Conversion-Etch" Mechanism Using Sequential Exposures of Hydrogen Fluoride and Trimethylaluminum. *Chem. Mater.* **2017**, *29*, 1183−1191.

(33) Weidlein, J.; Krieg, V. Vibrational Spectra of Dimethyl and Diethyl Aluminum Fluoride. *J. Organomet. Chem.* **1968**, *11*, 9−16.

(34) Min, K. S.; Kang, S. H.; Kim, J. K.; Jhon, Y. I.; Jhon, M. S.; Yeom, G. Y. Atomic Layer Etching of Al_2O_3 using BCl_3/Ar for the Interface Passivation Layer of III-V MOS Devices. *Microelectron. Eng.* **2013**, *110*, 457−460.

(35) Morrow, M. K. Synthesis and Characterization of Tetramethylhafnium. *Masters Thesis*; University of Tennessee: Knoxville, 1970; DOI: 10.2172/4153093.

(36) Berthold, H. J.; Groh, G. Preparation of Tetramethylzirconium $Zr(CH_3)_4$. *Angew. Chem., Int. Ed. Engl.* **1966**, *5*, 516.

DOI: 10.1021/acs.jpcc.9b04767
J. Phys. Chem. C 2019, 123, 18455−18466

(37) Lim, W. S.; Park, J. B.; Park, J. Y.; Park, B. J.; Yeom, G. Y. Low Damage Atomic Layer Etching of ZrO_2 by Using BCl_3 Gas and Ar Neutral Beam. *J. Nanosci. Nanotechnol.* **2009**, *9*, 7379−7382.
(38) Park, J. B.; Lim, W. S.; Park, B. J.; Park, I. H.; Kim, Y. W.; Yeom, G. Y. Atomic Layer Etching of Ultra-Thin HfO_2 Film for Gate Oxide in MOSFET Sevices. *J. Phys. D: Appl. Phys.* **2009**, *42*, No. 055202.

DOI: 10.1021/acs.jpcc.9b04767
J. Phys. Chem. C 2019, 123, 18455−18466